Europe PMC Funders Group
Author Manuscript

J Neuropathol Exp Neurol. Author manuscript; available in PMC 2015 February 20.

Published in final edited form as:
J Neuropathol Exp Neurol. 2010 October ; 69(10): 1017–1033. doi:10.1097/NEN.0b013e3181f3a5b1.

Europe PMC Funders Author Manuscripts

Europe PMC Funders Author Manuscripts

Activated microglia mediate axo-glial disruption that contributes to axonal injury in multiple sclerosis

Owain. W. Howell, PhD[#], **Jon. L. Rundle, PhD**[#], **Anurag Garg, BSc**, **Masayuki Komada, PhD**[1], **Peter. J. Brophy, PhD**[2], and **Richard Reynolds, PhD**
Centre for Neuroscience, Division of Experimental Medicine, Imperial College Faculty of Medicine, Hammersmith Hospital Campus, London W12 0NN

[1]Graduate School of Bioscience and Biotechnology, Tokyo Institute of Technology, Yokohama, 226-8501, Japan

[2]Centre for Neuro-regeneration, University of Edinburgh, Edinburgh EH16 4SB

[#] These authors contributed equally to this work.

Abstract

The complex symptoms of chronic multiple sclerosis (MS) are due, in part, to widespread axonal pathology affecting lesioned and non-lesioned areas of the CNS. Here we describe an association between microglial activation and axon/ oligodendrocyte pathology at nodal and paranodal domains in normal appearing white matter (NAWM) of MS and experimental allergic encephalomyelitis (EAE). The extent of paranodal axo-glial (neurofascin-155$^+$/Caspr1$^+$) disruption correlated with the local degree of microglial inflammation and axonal injury (expression of nonphosphorylated neurofilaments) in MS NAWM. These changes were independent of demyelinating lesions and did not correlate with the density of infiltrating lymphocytes. Similar axo-glial alterations were seen in pre-symptomatic EAE, at a time-point characterised by microglia activation prior to the infiltration of immune cells. Disruption of the axo-glial unit in adjuvant immunised animals was reversible and coincided with the resolution of microglial inflammation, whereas paranodal damage and microglial inflammation persisted in chronic EAE. We were able to preserve axo-glial integrity by administering minocycline, which inhibited microglial activation, in actively immunised animals. Therefore, permanent disruption to axo-glial domains in an environment of microglial inflammation is an early indicator of axonal injury that would affect normal nerve conduction contributing to pathology outside of the demyelinated lesion.

Keywords

Axon; demyelination; multiple sclerosis; neuroinflammation; neurofascin; sodium channel

---

Corresponding author: Dr. Owain Howell, Centre for Neuroscience, Division of Experimental Medicine, Burlington Danes research laboratories, Hammersmith Hospital Campus, Du Cane Road, London W12 0NN, Tel: (44) 020 7594 6657; Fax: (44) 020 7594 6548; o.howell@imperial.ac.uk.

Europe PMC Funders Author Manuscripts

Europe PMC Funders Author Manuscripts

Introduction

Multiple sclerosis (MS) is an inflammatory disease of the CNS that manifests as focal areas of inflammation, demyelination, gliosis and axon loss (1). Neurological decline in the progressive stages of MS is suggested to result from axon loss that is dependent on compartmentalised inflammation and chronic activation of the innate immune system (2), which is supported by the observation that progressive MS patients are refractory to therapies that target the peripheral immune component (3). The normal appearing white matter (NAWM) in progressive MS is often widely affected and contains areas of diffuse activated microglia, degenerating axons and a compromised blood brain barrier (4-6). Furthermore, imaging data also suggests that permanent neurological deficit may in part be attributed to these global and diffuse changes of the NAWM (7, 8).However, the nature and effects of this diffuse inflammation have been little studied.

The integrity of myelin producing oligodendrocytes is crucial for ensuring correct organisation of axonal domains required for action potential propagation and the maintenance of axon calibre and transport (9, 10). The glial 155kD isoform of neurofascin (Nfasc155) is expressed at the leading edge of the myelin sheath and associates with Caspr1 and contactin of the axolemma to ensure the correct generation and maintenance of paranodal axo-glial junctions and facilitate effective saltatory conduction (11-13). Nfasc155, Caspr1 or contactin single gene knockouts have disrupted axo-glial junctions and displaced K_V1 channels, which are normally expressed under the myelin sheath at the juxtaparanode. Such alterations in nodal architecture are accompanied by ataxia, muscle tremors and severely reduced nerve conduction velocities, despite normal myelin ensheathment (12-14).

Gene deletion of major oligodendrocyte and myelin proteins yields mice with morphologically normal myelin but with a striking axonal pathology, including organelle accumulation in nodal regions (15-17). The Nfasc155 null mouse lacks normal paranodal junctions and manifests an axonal pathology of disorganised neurofilaments and nodal/paranodal swellings (18), which suggest that changes to myelin composition or interruptions to glial-axonal communication can be catastrophic for normal axon function and survival.

Paranodal axo-glial components are lost earlier than nodal markers following myelin degeneration in rodents (19) and such changes are a sensitive indicator of early myelin abnormalities in MS (20-22). Here we report how changes in paranodal and nodal components are apparent in the MS NAWM and its murine model, at sites remote from lesions. These changes correlated with the incidence of activated microglia and suggest an important and novel mechanism of tissue injury in the inflamed CNS, whereby the disruption of axo-glial communication would impinge on normal saltatory conduction and normal axon function potentially contributing to the diversity of clinical symptoms.

Materials and methods

Human post-mortem tissue characterisation

Tissue for this study was provided by the UK Multiple Sclerosis Tissue Bank and the UK Parkinson’s Disease Society Tissue Bank at Imperial College London under ethical approval

Europe PMC Funders Author Manuscripts

Europe PMC Funders Author Manuscripts

from the National Research Ethics Committee (08/MRE09/31 and 07/MRE09/72). Eighteen cases of neuropathologically confirmed MS; (Table 1), 11 female; mean post-mortem delay (PMD) 17.2 hrs (range 7 - 24hrs); mean age 55.6 yrs (39 - 78 yrs); and mean disease duration 25.9 yrs (12 - 47yrs); six cases of PD, 3 female, PMD 20.2 hrs (range 15 – 28 hrs), mean age 79.2 yrs (75- 85 yrs) and mean disease duration 17.5 yrs (10- 27yrs); and 11 non-neurological controls; 3 female, mean post-mortem delay 22.4hrs (14 - 33hrs), mean age 71.9 yrs (35 - 88yrs) were used in this study. Tissue blocks (2×2×1cm) dissected immediately on brain retrieval were fixed in 4% paraformaldehyde (PFA, Sigma) in phosphate buffered saline (PBS) for a minimum of 12hrs, cryoprotected in 30% sucrose in PBS and cryosectioned at 10μm.

MS tissue blocks from frontal and parietal regions were characterised as normal appearing or lesional by screening with a panel of histochemical and immunohistological markers, as detailed previously (22). MS NAWM was defined as being at least 10mm from focal demyelinated plaques and avoiding neurofilament labelled fibre tracts emerging from grey/ white matter lesions. Briefly, all cases were processed for haematoxylin/ luxol fast blue (LFB) histology and immunohistochemistry/ immunofluorescence for HLA-DR, ionized calcium binding adapter molecule 1 (IBA1), myelin/ oligodendrocyte glycoprotein (MOG), glial fibrillary acidic protein (GFAP), neurofilament-H protein, and CD3 antigens (see supplementary table 1). PD tissue blocks containing subcortical white matter from frontal and parietal areas were screened for α-synuclein expression, microglial inflammation (HLA-DR$^+$, IBA1$^+$, CD68$^+$) and axonal pathology (neurofilament-H$^+$).

Induction of experimental allergic encephalomyelitis (EAE) in C57Bl/6 mice

Female C57Bl/6 mice (6-8 weeks; Charles River Laboratories) were immunised on days 0 and 7 with MOG$_{35\text{-}55}$ peptide (200μg; Advanced Biotechnology Centre, Imperial College London, UK) supplemented with incomplete Freunds adjuvant (IFA, Difco,MI) and 320μg *M. Tuberculosis,* 80μg *M. butyricum* (Difco, MI). Intraperitoneal (i.p) injections of pertussis toxin (200μg; Calbiochem, UK) were administered on days 0, 1, 7 and 8. MOG EAE, adjuvant controls (the absence of MOG peptide) and naives (n=5 per group) were weighed and assessed daily for clinical symptoms and all protocols for animal research conformed to UK Home Office Project Licence regulations.

Animals were terminally anesthetised and perfused intracardially with PBS followed by 4% PFA at day 10 (prior to disease onset) and day 44 (chronic disease). Spinal cords were post-fixed for 4hrs, cryoprotected in 30% sucrose in PBS and sectioned at 10μm. The spinal cord was cut into three pieces and the most rostral 3mm of each portion mounted for transverse sectioning and the remaining 10mm portions were sectioned longitudinally. Cellular infiltrates and myelin changes were assessed on the transverse and longitudinal sections of the spinal cord by immunostaining for CD3, CD11b, IBA1, iNOS, toll-like receptor 4 (TLR4), CD68 (ED1 antigen), neurofilament-H protein, nonphosphorylated neurofilaments (SMI32 antibody) and myelin basic protein (MBP). Quantification of CD11b immunoreactivity was performed on transverse sections (cervical, thoracic and lumbar) and paranodal/ nodal quantifications on lateral white matter tracts of the lumbar spinal cord.

Europe PMC Funders Author Manuscripts

Europe PMC Funders Author Manuscripts

Minocycline treatment

$MOG_{35\text{-}55}$ immunised animals (n=5) were administered minocycline hydrochloride i.p (Sigma) according to dosing regimen of Brundula et al. (23), from the day of EAE induction until the end of the experiment (day 13), when the first clinical signs were noted in vehicle animals and inflammation was widespread. Vehicle control animals (n=5) received saline at the same volume and frequency as the minocycline group. Spinal cord tissue was prepared as noted above.

Immunohistochemistry

Tissue sections were air dried, rehydrated in PBS and subjected to antigen retrieval when necessary (10mM sodium citrate buffer or methanol), before commencing with immunohistochemical or immunofluorescent staining protocols (22). All primary antibodies are listed in supplementary Table 1. Secondary antibodies were purchased from Vector Laboratories (Peterborough, UK), Molecular Probes (Invitrogen, Paisley, UK) and Jackson Immunoresearch (Stratech Scientific, Soham, Cambridgeshire, UK). Secondary antibody controls, processed using identical protocols except for the omission of primary antibodies, were devoid of staining.

Image analysis and Experimental details

Tissue sections were analysed on a Nikon E1000M epifluorescence microscope (Nikon Instruments Inc.) with a digital camera (QImaging) or by confocal laser scanning microscopy with a Leica SP5 MP inverted microscope (Leica Microsystems). All images were analysed using Image ProPlus (Media Cybernetics, Marlow, UK), and ImageJ (http://rsb.info.nih.gov/ij/) and prepared in Photoshop CS2 (Adobe Systems). Quantification was performed with the observer blinded to case identification.

Analysis of inflammation in MS NAWM—Microglial/ macrophage density and the incidence of damaged axons was assessed by quantifying HLA-DR^+ /$iNOS^+$ cells and $SMI32^+$ (nonphosphorylated $neurofilament^+$) axons from 4 randomly captured fields (200 × magnification; 0.07 mm^2) per region of NAWM per tissue block. Total perivascular and $CD3^+$ infiltrates were determined from a minimum of four (4-6) vascular structures per block. The perivascular space was outlined to calculate perivascular area and the number of $DAPI^+$ nuclei and the number of $CD3^+$/ $DAPI^+$ cells calculated per mm^2 of perivascular space. A composite measure of local inflammation and axonal stress was calculated using an empirical scoring system (0-10) in order to subgroup MS NAWM areas into low-level localised inflammation/axon pathology (MS low, 0-6) and high-level localised pathology (MS high, 7-10) for data comparisons with respect to K_v1 distribution. The scoring was based on numbers of HLA-DR^+ process bearing microglia (0= 0-100 cells/ mm^2; 1= 101-200; 2= 200+ cells), the absence or presence of microglial nodules (0= none; 1= nodules present) and parenchymal amoeboid HLA-DR^+ macrophages (0= none; 1=present – albeit at very low densities of 1-2 cells per field), perivascular $CD3^+$ T-cells (0= 0-500/ mm^2; 1= 501-1000; 2= 1001+), $iNOS^+$ cells (0= 0-100; 1= 101-200; 2= 200+) and $SMI32^+$ axons (0= 0-10; 1= 11-20; 2= 20+/ mm^2).

Europe PMC Funders Author Manuscripts

Europe PMC Funders Author Manuscripts

Quantifying disruption of the node of Ranvier—Nodal, paranodal and juxtaparanodal domains were measured based on the extent of pan-Na_v1, $Na_v1.6$, βIV spectrin, Nfasc155, Caspr1 or $K_v1.2$ expression on fluorescent images of regions of interest (ROI) scored for inflammation. Images were captured with a 63× oil-immersion objective (captured field =0.008mm^2) and only positive paranodal structures in focus were measured from a minimum of 8 sampled fields (8-14) per ROI for each tissue block analysed. Mean ± SEM values were calculated per ROI and the group means (e.g. Control, MS) plotted with PRISM (GraphPad Software Inc.) as bar graphs or box plots (showing median, 25-75% data and whiskers that represent the minimum and maximum observation). Groups were compared using non-parametric Mann Whitney t-test or ANOVA and appropriate post test (PRISM) as noted in the figure legends.

Data were plotted as single paranode length, nodal length (the unstained region between Nfasc155$^+$ paranodes), and Nfasc155$^+$ paranodal width per experimental group. To investigate the association between Nfasc155$^+$ paranodal profiles and axonal damage, the length of Nfasc155$^+$ profiles associated with SMI32$^+$ axons was assessed. Nfasc155$^+$ structures on SMI32$^+$ axons were compared to adjacent profiles not associated with SMI32$^+$ fibres. Nodes were analysed by measuring the axonal length of pan-Na_v1^+ profiles from Na_v1^+/ Nfasc155$^+$ co-labelled sections. Changes at the juxtaparanodal/paranodal domain were assessed by quantifying the number of overlapping $K_v1.2^+$/ Nfasc155$^+$ domains and the distance separating the juxtaparanode and node of Ranvier. The number of normal appearing $Na_v1.6^+$ nodes (strong $Na_v1.6$ immunoreactivity flanked by Nfasc155$^+$ expression) and the combined frequency of aberrant nodes (nodes with no detectable $Na_v1.6$ reactivity or the presence of “split” or heminodal $Na_v1.6^+$ associated with Nfasc155$^+$ staining) was calculated and expressed as percentage of total nodes quantified. To determine the aberrant nature of nodal $Na_v1.6$ expression in EAE spinal cord, z-stacks of images from areas of interest were captured from actively immunised mice at dpi 10 (n=3 animals). A line selection of constant length was centred to the node and the intensity of Nfasc155 and $Na_v1.6$ signal determined using a modified version of the RGB profiles tool (http://rsb.info.nih.gov/ij/macros/tools/RGBProfilesTool.txt) courtesy of Dr.C. Liebig, Imperial College London (http://www3.imperial.ac.uk/imagingfacility/resources).

Results

Paranodal axo-glial junctions are disrupted in MS normal appearing white matter and Parkinson’s disease white matter

We were interested in examining changes to the axo-glial complex in MS NAWM and how it might be affected by local inflammation in comparison to subcortical white matter from non-neurological, age-matched controls (Fig. 1). To determine the specificity of the structural alterations to these domains, we also studied PD brain tissue blocks that contained diffuse microglial inflammation without demyelination (see supplementary Fig. 1).

Regions of NAWM were carefully selected for analysis of inflammation and nodal/ paranodal alterations from fixed-frozen and cryosectioned blocks of superior frontal and/ or parietal subcortical white matter (Fig. 1). LFB histology and immunostaining for MOG proteins confirmed myelin integrity (Fig. 1A,B). NAWM typically contained scattered

Europe PMC Funders Author Manuscripts

Europe PMC Funders Author Manuscripts

HLA-DR$^+$ microglia with an activated morphology (thicker and shorter processes compared to control microglia; Fig. 1C), very few amoeboid macrophages and T-lymphocytes restricted to perivascular sites (Fig. 1D). SMI32$^+$ axons displaying localised swellings and transections associated with ramified microglia, which frequently expressed iNOS (Fig. 1E, F). Microglial activation (activated morphology and increased expression of IBA1) was increased in MS NAWM in comparison to age-matched non-neurological control samples (Fig. 1G, H). Immunostaining NAWM areas of interest for components of paranodal axo-glial junctions such as Nfasc155$^+$, normally reveals discreet pairs of structures separated by Na_V 1$^+$ channels at the node (Fig. 2A). Elongated and disrupted Nfasc155$^+$ paranodes were seen in MS NAWM and PD that contrasted with the more regular, discrete pattern of paired Nfasc155$^+$ paranodes normally seen (MS example, Fig. 2A, B; PD example, supplementary Fig. 1). Double-immunofluorescence for Nfasc155$^+$ in the glial end loops and Caspr1 in the axolemma revealed elongated paranodes with a disrupted profile, identical for both proteins (Fig. 2C, D). The co-localisation of Nfasc155 and Caspr1 means that either protein can be used as an indicator of changes at paranodal axo-glial junctions, and implies that both oligodendrocyte and axonal compartments are similarly affected. To confirm that paranodal junctions were altered in MS we measured the axonal length and width of single Nfasc155$^+$ structures and the length of the unstained nodal gap between pairs of Nfasc155$^+$ paranodes. In total, 928 individual Nfasc155$^+$ paranodal profiles from 18 cases of neuropathologically confirmed MS and 583 paranodes from 11 cases of non-neurological controls were quantified and plotted as mean paranodal length/ case (Fig. 2 E). Nfasc155$^+$ paranodal length was 23% longer on average in the MS NAWM (2.9± 0.1μm, Fig. 2E; $p< 0.001$) in comparison to non-neurological controls (2.3± 0.1μm). Almost a fifth of all quantified Nfasc155$^+$ structures in MS (170 of 928; 18%) were longer than the 95th percentile of quantified control paranodes (2.74μm). In contrast, the length of the nodes of Ranvier (1.4± 0.17 and 1.61± 0.06μm) and the width of Nfasc155$^+$ paranodes (0.75± 0.07 and 0.89± 0.02μm) were unchanged between control and MS subjects, respectively.

Tissue pathology and microglial activation can be affected by confounding agonal and post-mortem events. For the cases used in this study we found no correlation between post-mortem delay, age or cause of death with our measures of paranodal integrity, microglial activation and axonal pathology (see supplementary Table. 2).

The degree of paranodal axo-glial disruption correlates with microglial inflammation in multiple sclerosis

To examine the relationship between WM inflammation and paranodal alterations in MS, we quantified the numerical density of microglia, macrophages, iNOS$^+$ cells, and CD3$^+$ T-cells within the same fields of NAWM used for quantification of Nfasc155$^+$ paranodal profiles. A significant positive correlation was seen between the mean Nfasc155$^+$ paranodel length and the density of HLA-DR$^+$ ramified microglia and iNOS$^+$ microglia (Fig. 2F, G). In contrast, paranodal disruption did not correlate with the presence of total perivascular infiltrates (data not shown) or the number of perivascular CD3$^+$ T-cells (Fig. 2H), indicating an influence of local microglial inflammation rather than peripheral immune infiltrates on paranodal integrity.

Europe PMC Funders Author Manuscripts

Europe PMC Funders Author Manuscripts

Disrupted paranodes are associated with SMI32$^+$ stressed/damaged axons

Paranodal disruption was greatest in those cases with the highest density of SMI32$^+$ stressed/ damaged axons ($p < 0.001$; Fig. 3A). The majority of disrupted and elongated Nfasc155$^+$ profiles were directly associated with SMI32$^+$ axons in the MS NAWM (forty of 52 paranodes with a length greater than the 75 percentile were associated with SMI32$^+$ axons). Nfasc155$^+$ paranodes were significantly elongated on SMI32$^+$ (paranode length, 4± 0.2μm) in comparison to paranodes associated with SMI32$^-$ axons (2.8± 0.1μm; Fig. 3B, C). SMI32$^+$ axons in control tissues (albeit at a much reduced density in comparison to MS) were also associated with alterations in Nfasc155$^+$ paranodal domains (2.3± 0.1μm and 2.9± 0.1μm, for Nfasc155$^+$ profiles associated with SMI32$^-$ and SMI32$^+$ axons in control tissues), indicating the close relationship between neurofilament phosphorylation and axo-glial junction integrity. SMI32$^+$ axonal swellings were noted at disrupted nodes (Fig. 3D) and accumulations of amyloid precursor protein (APP) occasionally associated with disrupted nodal profiles in the NAWM (Fig. 3E), supporting previous reports of nodal/paranodal domains as frequent sites of early axonal pathology (10).

Juxtaparanodal disruption is accompanied by increased microglial inflammation

A primary role of the organised paranodal axo-glial junction is the segregation of the ion channel rich domains of the node and juxtaparanode, which become displaced upon disruption of the paranode. To determine if the elongated NFasc155$^+$ paranodal profiles represented disrupted structures and if this was associated with local inflammation, we examined the distribution of nodal (pan Na$_V$1$^+$) and juxtaparanodal (K$_V$1.2$^+$) domains in NAWM tissue with low or high levels of inflammation (see methods and Table 1) in comparison to controls (Fig. 4). A significant displacement of K$_V$1$^+$ domains closer to the node of Ranvier was observed in MS NAWM. The displacement was greatest in the MS group with the most pronounced inflammation in the NAWM (separation from node to juxtaparanode for control= 4.6± 0.2μm; MS low= 4.2± 0.2μm and MS high= 3.7± 0.1μm; Fig. 4D). The occurrence of overlapping Nfasc155$^+$/ K$_V$1$^+$ domains was also greatest in this group (percent overlapping juxtaparanodal/ paranodal domains for control= 10.8%, MS low= 34.6% and MS high= 46%; Fig. 4E).

Quantification of Na$_V$1$^+$ nodal profiles (Fig. 4F) revealed these structures to be unchanged in size between control and MS. These data are in agreement with our earlier observations of an unchanged nodal gap between paired Nfasc155$^+$ paranodes (see above). Na$_V$1.6 channels are the primary Na$_V$1 component of mature nodes and are tethered at the axolemma through interactions with axonal neurofascin (Nfasc186), contactin, ankyrin G and βIV spectrin (24). Immunolabelling revealed the overwhelming majority of Nfasc155$^+$ paranodal axo-glial junctions to be associated with βIV spectrin$^+$ (Fig. 4G-I) or Na$_V$1$^+$ (Fig. 2A,B,E) nodes, although the expression of Na$_V$ 1.6 was attenuated and sometimes undetectable between Caspr1$^+$ paranodes (Fig. 4J-L).

Microglial activation is apparent before onset of clinical disease in experimental autoimmune encephalomyelitis

To study the relationship between inflammation and paranodal disruption we used a murine autoimmune model that mimics some of the features of MS pathology (25). Microglial

Europe PMC Funders Author Manuscripts

activation, quantified by the area of CD11b immunoreactivity in transverse sections of spinal cord, was increased in MOG immunised animals at 10 days post-induction (dpi) and in long term CFA and MOG groups at 44 dpi (Fig. 5A, B). At 10 dpi in MOG EAE, before the appearance of clinical symptoms and the influx of peripheral immune cells, CD11b immunoreactivity was increased and double immunofluorescence for iNOS and TLR4 indicated the presence of reactive microglia in a perivascular location and in the parenchyma of the lumbar spinal cord white matter (Fig. 5C). Adjuvant-only (CFA dpi 10) animals contained activated ($TLR4^+$/ $IBA1^+$) microglia which were not noted in long term CFA animals indicating their activation state, assessed by TLR4 expression, to be reduced (Fig. 5D,E), although CD11b immunoreactivity was increased ($p<0.01$; Fig. 5B). By analysing paranodal changes at 10dpi after immunisation with MOG we were able to study the effects of microglial activation on the integrity of the axo-glial unit in the absence of parenchymal lymphocytic infiltration and demyelination.

Disruption of $Nfasc155^+$ paranodes in MOG and CFA immunised animals

In presymptomatic MOG immunised mice at 10 dpi, discrete and elongated $Nfasc155^+$ paranodes were noted in the lateral lumbar spinal cord (some distance from potentially confounding meningeal infiltrates; Fig. 5F). Measurement of paranodal length, width and nodal gap in MOG EAE mice revealed the significant elongation of $Nfasc155^+$ paranodes by 10 dpi (3.0± 0.03μm; 17% longer than controls, 2.6± 0.1μm), which further increased in long term MOG immunised animals (4.3± 0.2μm; 67% longer). Surprisingly, CFA control immunised animals at 10 dpi not only exhibited microglial activation ($TLR4^+$) but also had significantly elongated paranodal profiles (3.1± 0.1μm). However, paranodal disruption in the CFA immunised group appeared transient as $Nfasc155^+$ paranodal length returned to control levels in the long term animals (Fig. 4G), when microglial TLR4 expression had resolved. In agreement with our data from the human tissue, paranodal $Nfasc155^+$ width and the length of the unstained nodal gap between pairs of $Nfasc155^+$ structures were unchanged in all groups compared to naïve controls (data not shown).

$Nfasc155^+$ paranodal disruption in EAE is associated with juxtaparanodal re-arrangements and axonal stress

$Nfasc155^+$ paranodal elongation in MOG immunised animals is likely to be indicative of a disrupted axo-glial junction as it was accompanied by encroachment of juxtaparanodal $K_V1.2$ channels towards the node with significantly increased incidence of overlapping $K_V1.2^+$/$Nasfc155^+$ expression in both MOG (38.3% ± 2.5; $p<0.001$) and CFA (28.9 ± 0.6; $p<0.05$) immunised animals in comparison to naïve controls (Fig. 6A,B,D). There was evidence of $SMI32^+$ axons in both experimental groups and these were associated with $Nfasc155^+$ paranodes with an elongated phenotype (Fig. 6C,E). In MOG immunised animals, paranodal length was 32% greater for paranodes associated with $SMI32^+$ axons (3.0± 0.2μm) in comparison to those not associated with $SMI32^+$ axons (2.3± 0.1μm). A similar relationship was found for CFA animals (Fig. 6E). Therefore, at pre-symptomatic stages before demyelination occurs, axonal stress and microgliosis are accompanied by paranodal axo-glial alterations similar to that seen in MS NAWM.

Europe PMC Funders Author Manuscripts

Europe PMC Funders Author Manuscripts

Disruption of nodal expression of voltage-gated sodium channels

We noticed that disrupted paranodes were often accompanied by changes in the composition (Na_V1 channel subtype), but not morphology, of nodes in both MS NAWM and EAE (Fig. 4, 7). In order to determine how nodal components were affected in early disease in relation to changes at the paranodal axo-glial junction, we investigated the expression of $Na_V1.6$ channel subtype in combination with Nfasc155 expression. Paranodes were almost always separated by βIV spectrin$^+$ nodes (see Fig. 7A; βIV spectrin$^+$ nodes per pair of caspr1$^+$ paranodes from naive (94± 1%) and MOG immunised animals (95± 1%), respectively; 1070 paranodes examined) and pan Na_V1 (Na_V1^+ nodes per Nfasc155$^+$ paranodes in naïve (94± 1%) and MOG immunised animals (95± 1%), respectively; 800 paranodes examined). In contrast, numerous instances of $Na_V1.6$ negative nodes were seen (Fig. 7B-E). Confocal analyses of image stacks were used to generate line histograms of signal intensity through the nodal region to reveal this to be a true loss of detectable $Na_V1.6$ immunoreactivity at these nodes (Fig. 7F, G). We measured the number of normal appearing nodes (strong $Na_V1.6$ immunoreactivity (Fig. 7C) and the combined frequency of nodes with no $Na_V1.6$ reactivity (Nav1.6 negative nodes) or abnormal morphology, in association with Nfasc155$^+$ structures. At 10 dpi both MOG and CFA immunised animals had a reduction in the number of normal appearing nodes compared to naïve (27% and 33.3% reduction, respectively; Fig. 7H,I). At 44 dpi MOG immunised animals showed a significant reduction in normal appearing $Na_V1.6^+$ nodes compared with naive (46.4% reduction). The loss of $Na_V1.6$ expression in CFA animals at 10 dpi was reversed at 44 dpi, indicating the transient nature of nodal/ paranodal abnormalities in the absence of a prolonged antigenic stimulus and microglial activation (Fig 5).

Minocycline reduces microglial activation and nodal/ paranodal disruption

Our human post-mortem tissue and EAE results suggest that microglial activation is responsible for the paranodal and nodal alterations associated with axonal pathology. To test this hypothesis, we examined paranodal and nodal domains in MOG immunised mice that had been treated with minocycline, a potent inhibitor of systemic and CNS inflammation. Following 13 days of prophylactic minocycline treatment (when vehicle-MOG animals first displayed symptoms), microglia had a resting morphology (Fig. 8D-H) and the density of CD11b immunoreactivity (Fig. 8A-C; 4.87±0.3%) was significantly reduced in minocycline dosed animals in comparison to vehicle-MOG controls (11.4±2.4%). Therefore, peripheral administration of minocycline was effective in reducing the level of CNS parenchymal inflammation at this timepoint.

Average paranodal length in minocycline treated animals (2.87±0.58) was reduced in comparison to vehicle controls (3.55±1.2; Fig. 7F), to a level comparable to that of naïve animals (Fig. 5G). Minocycline treated animals displayed a significantly greater expression of nodal $Na_V1.6^+$ associated with Nfasc155$^+$ paranodes (75.3%±4.1) compared to vehicle-MOG animals (65%±5; Fig. 8I). These data demonstrate that an attenuation of inflammation is sufficient to reduce nodal/ paranodal pathology in vivo.

Europe PMC Funders Author Manuscripts

Discussion

We have demonstrated that disruption of paranodal and nodal domains correlates with axonal pathology and the degree of local microglial inflammation in MS NAWM and EAE spinal cord and suggest that this could provide a novel mechanism of tissue injury in acute and chronic CNS disease states. Such molecular alterations would be expected to: 1) disrupt normal neurotransmission along the affected fibres; 2) disrupt axo-glial communication; 3) disrupt the axonal cytoskeleton, thereby affecting normal axon transport, and 4) expose novel targets to immune attack that could further exacerbate damage to the axon or ensheathing oligodendrocyte.

Paranodal/ nodal disruption is closely associated with axonal pathology

Paranodal disruption manifests as a loss of the electron dense transverse bands believed to represent the protein-protein interactions of the axo-glial unit with a concomitant widening of the axo-glial space (12, 13, 26). The increased separation at the axo-glial junction is accompanied by an elongation of the longitudinal paranodal profile, as shown by alterations in Nfasc155$^+$ and Caspr1$^+$ immunostaining. This could represent the progressive loss or disrupted contact of the innermost turns of the myelin sheath, as seen in the Nfasc155 null mouse (18), which is accompanied by encroachment of juxtaparanodal constituents into paranodal domains, as the molecular fence to protein diffusion is removed (27). A greater incidence of juxtaparanodal K_V1^+ in Nfasc155$^+$ domains was noted in both MS and EAE tissues, which would indicate paranodal sealing to be reduced, with predictable consequences for nerve conduction dynamics.

In the current study disrupted Nfasc155$^+$ paranodes were nearly always associated with stressed/ damaged axons, visualised by immunostaining with the SMI32 antibody that is a marker of early axonal pathology in MS, Alzheimer's and ALS (28, 29). Although it is not possible to determine the relative timing of paranode disruption and that of neurofilament dephosphorylation in the post-mortem material, the frequency of Nfasc155$^+$/ SMI32$^+$ structures suggests that such changes may occur concurrently. How might axo-glial disruption be concurrent with axon damage? Nfasc155 is required for the proper targeting of Caspr1/ contactin to the axonal membrane and together they form protein complexes stabilised by interactions with the axon cytoskeleton via the cytoplasmic tail of Caspr1 bound to protein 4.1B (11, 30). Ankyrin B, 4.1B and αII- and βII-spectrin accumulate subsequent to Caspr1, generating a specialised cytoskeleton at the paranode that may be linked to axonal neurofilaments (31). Therefore, axo-glial disruption may be the cause or the consequence of axonal paranodal cytoskeletal alterations that associate with localised pathology (32). Consistent with this, axonal swellings occur at the node in the Nfasc155 null animal (18) and we noted many SMI32$^+$ focal swellings and end bulbs, together with accumulations of APP at nodal regions, indicating alterations in the axon cytoskeleton and normal fast transport in areas of paranodal disruption.

Paranodal disruption as a consequence of microglial inflammation

The pathology of NAWM is a consequence of microglial activation, lymphocyte infiltration, myelin damage and axonopathy (6, 33-36). Activated microglia contribute to the

Europe PMC Funders Author Manuscripts

Europe PMC Funders Author Manuscripts

inflammatory milieu by the secretion of cytokines, free radicals, and sustain inflammation by presenting antigen to circulating lymphocytes (37). We confirmed the presence of reactive microglia based on their activated morphology and expression of markers induced by pro-inflammatory cues (38). Microglial/ macrophage derived glutamate is one important mediator of cell damage in MS (39). Extracellular glutamate causes paranodal disruption, juxtaparanodal rearrangements and eventual axonal degeneration (40).

Although there was no correlation between perivascular T-cell infiltrates and changes in Nfasc155 expression, it is likely that T-cell infiltrates, which are a hallmark of progressive MS (6), could sustain parenchymal inflammation thereby indirectly affecting axo-glial domains. It may also be argued that axonal pathology caused by distant lesions might lead to axo-glial disruption in the NAWM. By visualising myelin and axons using immunochemistry we ensured sampled NAWM did not contain axons emanating from lesions from the same tissue block, but due to the heterogeneity of lesion sites we cannot be completely sure that sampled axons had not been damaged as a consequence of a distant demyeliating event. Nevertheless, in nearly all instances of paranodal alterations that associated with underlying axonal stress ($SMI32^+$), the pattern of axonal nonphosphorylated neurofilament expression was immediate with the affected paranodes, suggesting that the majority of axonal changes were local to the site of paranodal dysfunction. The inclusion of PD disease tissue in our studies enabled us to study a disease characterised by microglial inflammation without the confounding effects of near or distant demyelinated lesions, whilst neuropathology at the nodal unit in MOG EAE at a time-point before demyelination had occurred, also supports our hypothesis of a local microglial derived pathology of axo-glial signalling.

Significant neuropathology is apparent before the onset of clinical symptoms in the course of $MOG_{35\text{-}55}$ induced EAE (41-43). This is in part due to the presence of TLR ligands (e.g pertussis toxin and mycobacteria) in the adjuvant that can stimulate pro-inflammatory signalling and microglial inflammation (44, 45), which are vital for disease induction. The pre-symptomatic inflammatory response within the CNS is initiated by the early induction of the innate immune system, which precedes the influx of peripheral immune cells (46). Changes in the expression of pro-inflammatory genes such as CD11b, myeloperoxidase and cyclo-oxygenase-2 are noted as early as dpi 3, and occur to a similar extent in $MOG_{35\text{-}55}$ immunised and CFA-only animals. Changes in pro-inflammatory gene expression were also noted in $Rag^{-/-}$ mice that lack the adaptive arm of the immune system due to the absence of B- and T-lymphocyes (46). We have shown the pathology of $MOG_{35\text{-}55}$ immunised animals at 10 dpi, before the influx of inflammatory cells, was characterised by the activation of microglia ($iNOS^+$, $TLR4^+$) that was associated with axo-glial disruption and axonal injury. Similar but transient changes in nodal/ paranodal domains were noted in CFA-only treated animals, supporting the theory that an activated innate immune system is the likely pathological source of toxic factors in the CNS capable of disrupting these domains at this early time-point. In the absence of a sustaining CNS antigen (no MOG peptide) in the long term CFA group, microglial expression of TLR4 resolved, and this ‘resting’ phenotype was associated with nodal domains unchanged in comparison to age-matched naïve animals. These *in vivo* observations suggest that pro-inflammatory activation of microglia is

Europe PMC Funders Author Manuscripts

Europe PMC Funders Author Manuscripts

sufficient to induce nodal/ paranodal abnormalities and associated axonal pathology. Minocycline has a complex pharmacology and inhibits CNS inflammation through direct effects on resident microglia/macrophages and on the peripheral immune system by inhibiting the activation of auto-reactive T cells (47-49). In the present study, minocycline reduced microglial density and nodal/ paranodal disruption. This experiment provides further evidence for the damaging potential of inflammation at nodal and paranodal domains.

Reduced expression of Na_V1.6 at affected nodes

Maintenance of the correct molecular architecture of the node of Ranvier is vital for continued rapid propagation of electrical impulses (24). Myelination, and the formation of paranodal axo-glial junctions, is important for the transition from Na_V1.2 to Na_V1.6 as nodes mature (50, 51), and reduced expression of Nav1.6 results in slowed conduction (52, 53). The large majority of myelinated nodes in MS NAWM expressed βIV spectrin and immunostained with the panNa_V1 marker. Nevertheless, we noted numerous instances of $Na_V1.6^+$ negative nodes between paranodes, analogous to that reported in experimental allergic neuritis that correlate with a reduced nerve conduction (54). The loss of detectable Na_V1.6 was investigated in pre-symptomatic and long term EAE, where a significant proportion of white matter nodes lacked measurable Na_V1.6 expression. These changes persisted in MOG immunised animals with chronic disease but were not seen in the long term CFA controls, suggesting that the regulation of Na_V1.6 expression at the node could be directly affected by the inflammatory milieu. Loss of the major Na_V1 channel at nodes, disruption of paranodal axo-glial junctions and displacement of K_V1 channels would be expected to contribute to changes in nerve conduction along affected axons in this disease, which would warrant further investigation.

Changes at the paranodal axo-glial junction may be an early marker of cell stress and a precursor to demyelination and neurodegeneration

Subtle myelin abnormalities in the MS NAWM may allow T-cell or antibody mediated attack to occur more readily by the exposure of internodal oligodendrocyte and axonal membranes to the inflammatory milieu. Such a scenario is supported by data from the PLP overexpressing rat, which exhibits exacerbated EAE disease facilitated by the mild microglial inflammation and unstable myelin that is a hallmark of these animals (55). Furthermore, autoimmunity to neurofascin and contactin2 have recently been described in some MS patients (56, 57), and it is conceivable that the accessibility of such antigens would be enhanced in areas of paranodal abnormalities.

Demyelinated axons in MS are vulnerable to further injury culminating in their destruction. The denuded axon, in an attempt to restore conduction, re-expresses Na_V along its membrane (58, 59) contributing to an elevated energy demand on a structure exposed to damaging inflammation that is likely to result in its degeneration (reviewed by (60). Therefore, in addition to expected effects on saltatory conduction, changes at the paranode in the presence of activated microglia could be the prelude to demyelination and neurodegeneration in a number of pathological scenarios, contributing to an array of diffuse clinical symptoms.

Europe PMC Funders Author Manuscripts

Europe PMC Funders Author Manuscripts

Supplementary Material

Refer to Web version on PubMed Central for supplementary material.

Acknowledgements

All tissue samples were supplied by the UK Multiple Sclerosis Tissue Bank (www.ukmstissuebank.imperial.ac.uk/) and the Parkinson's Disease Tissue Bank (www.parkinsonstissuebank.org.uk). This study was funded by the Medical Research Council (G0700356 to OH and RR). We thank Dr. P. McIntosh (Department of neuroinflammation, University College London) for helpful discussions and Dr. C. Liebig (Facility for Imaging by Light Microscopy, Imperial College London), for expert assistance.

References

1. Lassmann, H.; Wekerle, H.; Compston, A.; Confavreux, C.; McDonald, I.; Miller, DH.; Noseworthy, JH.; Smith, KJ. The pathology of Multiple Sclerosis. McAlpine's Multiple Sclerosis. 4th. Churchill Livingstone; London: 2005. p. 557-99.
2. Weiner HL. A shift from adaptive to innate immunity: a potential mechanism of disease progression in multiple sclerosis. J Neurol. 2008; 255(Suppl 1):3–11. [PubMed: 18317671]
3. Compston A, Coles A. Multiple sclerosis. Lancet. 2008; 372:1502–17. [PubMed: 18970977]
4. Kirk J, Plumb J, Mirakhur M, McQuaid S. Tight junctional abnormality in multiple sclerosis white matter affects all calibres of vessel and is associated with blood-brain barrier leakage and active demyelination. J Pathol. 2003; 201:319–27. [PubMed: 14517850]
5. Plumb J, McQuaid S, Mirakhur M, Kirk J. Abnormal endothelial tight junctions in active lesions and normal-appearing white matter in multiple sclerosis. Brain Pathol. 2002; 12:154–69. [PubMed: 11958369]
6. Kutzelnigg A, Lucchinetti CF, Stadelmann C, Bruck W, Rauschka H, Bergmann M, Schmidbauer M, Parisi JE, Lassmann H. Cortical demyelination and diffuse white matter injury in multiple sclerosis. Brain. 2005; 128:2705–12. [PubMed: 16230320]
7. Filippi M, Tortorella C, Bozzali M. Normal-appearing white matter changes in multiple sclerosis: the contribution of magnetic resonance techniques. Mult Scler. 1999; 5:273–82. [PubMed: 10467388]
8. Ciccarelli O, Werring DJ, Wheeler-Kingshott CA, Barker GJ, Parker GJ, Thompson AJ, Miller DH. Investigation of MS normal-appearing brain using diffusion tensor MRI with clinical correlations. Neurology. 2001; 56:926–33. [PubMed: 11294931]
9. Edgar JM, Nave KA. The role of CNS glia in preserving axon function. Curr Opin Neurobiol. 2009; 19:498–504. [PubMed: 19765974]
10. Nave KA, Trapp BD. Axon-glial signaling and the glial support of axon function. Annu Rev Neurosci. 2008; 31:535–61. [PubMed: 18558866]
11. Sherman DL, Tait S, Melrose S, Johnson R, Zonta B, Court F, Macklin WB, Meek S, Smith AJH, Cottrell DF, Brophy PJ. Neurofascins Are Required to Establish Axonal Domains for Saltatory Conduction. Neuron. 2005; 48:737–42. [PubMed: 16337912]
12. Bhat MA, Rios JC, Lu Y, Garcia-Fresco GP, Ching W, St Martin M, Li J, Einheber S, Chesler M, Rosenbluth J, Salzer JL, Bellen HJ. Axon-glia interactions and the domain organization of myelinated axons requires neurexin IV/Caspr/Paranodin. Neuron. 2001; 30:369–83. [PubMed: 11395000]
13. Boyle ME, Berglund EO, Murai KK, Weber L, Peles E, Ranscht B. Contactin orchestrates assembly of the septate-like junctions at the paranode in myelinated peripheral nerve. Neuron. 2001; 30:385–97. [PubMed: 11395001]
14. Zonta B, Tait S, Melrose S, Anderson H, Harroch S, Higginson J, Sherman DL, Brophy PJ. Glial and neuronal isoforms of Neurofascin have distinct roles in the assembly of nodes of Ranvier in the central nervous system. J Cell Biol. 2008; 181:1169–77. [PubMed: 18573915]

Europe PMC Funders Author Manuscripts

Europe PMC Funders Author Manuscripts

15. Griffiths I, Klugmann M, Anderson T, Yool D, Thomson C, Schwab MH, Schneider A, Zimmermann F, McCulloch M, Nadon N, Nave KA. Axonal Swellings and Degeneration in Mice Lacking the Major Proteolipid of Myelin. Science. 1998; 280:1610–3. [PubMed: 9616125]
16. Lappe-Siefke C, Goebbels S, Gravel M, Nicksch E, Lee J, Braun PE, Griffiths IR, Nave KA. Disruption of Cnp1 uncouples oligodendroglial functions in axonal support and myelination. Nat Genet. 2003; 33:366–74. [PubMed: 12590258]
17. Edgar JM, McLaughlin M, Yool D, Zhang SC, Fowler JH, Montague P, Barrie JA, McCulloch MC, Duncan ID, Garbern J, Nave KA, Griffiths IR. Oligodendroglial modulation of fast axonal transport in a mouse model of hereditary spastic paraplegia. J Cell Biol. 2004; 166:121–31. [PubMed: 15226307]
18. Pillai AM, Thaxton C, Pribisko AL, Cheng JG, Dupree JL, Bhat MA. Spatiotemporal ablation of myelinating glia-specific neurofascin (Nfasc NF155) in mice reveals gradual loss of paranodal axoglial junctions and concomitant disorganization of axonal domains. J Neurosci Res. 2009; 87:1773–93. [PubMed: 19185024]
19. Mathis C, Denisenko-Nehrbass N, Girault JA, Borrelli E. Essential role of oligodendrocytes in the formation and maintenance of central nervous system nodal regions. Development. 2001; 128:4881–90. [PubMed: 11731467]
20. Wolswijk G, Balesar R. Changes in the expression and localization of the paranodal protein Caspr on axons in chronic multiple sclerosis. Brain. 2003; 126:1638–49. [PubMed: 12805111]
21. Coman I, Aigrot MS, Seilhean D, Reynolds R, Girault JA, Zalc B, Lubetzki C. Nodal, paranodal and juxtaparanodal axonal proteins during demyelination and remyelination in multiple sclerosis. Brain. 2006; 129:3186–95. [PubMed: 16766541]
22. Howell OW, Palser A, Polito A, Melrose S, Zonta B, Scheiermann C, Vora AJ, Brophy PJ, Reynolds R. Disruption of neurofascin localization reveals early changes preceding demyelination and remyelination in multiple sclerosis. Brain. 2006; 129:3173–85. [PubMed: 17041241]
23. Brundula V, Rewcastle NB, Metz LM, Bernard CC, Yong VW. Targeting leukocyte MMPs and transmigration: minocycline as a potential therapy for multiple sclerosis. Brain. 2002; 125:1297–308. [PubMed: 12023318]
24. Salzer JL. Polarized domains of myelinated axons. Neuron. 2003; 40:297–318. [PubMed: 14556710]
25. Gold R, Linington C, Lassmann H. Understanding pathogenesis and therapy of multiple sclerosis via animal models: 70 years of merits and culprits in experimental autoimmune encephalomyelitis research. Brain. 2006; 129:1953–71. [PubMed: 16632554]
26. Dupree JL, Girault JA, Popko B. Axo-glial interactions regulate the localization of axonal paranodal proteins. JCell Biol. 1999; 147:1145–52. [PubMed: 10601330]
27. Pedraza L, Huang JK, Colman DR. Organizing principles of the axoglial apparatus. Neuron. 2001; 30:335–44. [PubMed: 11394997]
28. Trapp BD, Peterson J, Ransohoff RM, Rudick R, Mork S, Bo L. Axonal Transection in the Lesions of Multiple Sclerosis. The New England Journal of Medicine. 1998; 338:278–85. [PubMed: 9445407]
29. Petzold A. Neurofilament phosphoforms: surrogate markers for axonal injury, degeneration and loss. J Neurol Sci. 2005; 233:183–98. [PubMed: 15896809]
30. Denisenko-Nehrbass N, Oguievetskaia K, Goutebroze L, Galvez T, Yamakawa H, Ohara O, Carnaud M, Girault JA. Protein 4.1B associates with both Caspr/paranodin and Caspr2 at paranodes and juxtaparanodes of myelinated fibres. EurJ Neurosci. 2003; 17:411–6. [PubMed: 12542678]
31. Garcia-Fresco GP, Sousa AD, Pillai AM, Moy SS, Crawley JN, Tessarollo L, Dupree JL, Bhat MA. Disruption of axo-glial junctions causes cytoskeletal disorganization and degeneration of Purkinje neuron axons. ProcNatl AcadSciUSA. 2006; 103:5137–42.
32. Einheber S, Bhat MA, Salzer JL. Disrupted Axo-Glial Junctions Result in Accumulation of Abnormal Mitochondria at Nodes of Ranvier. Neuron Glia Biol. 2006; 2:165–74. [PubMed: 17460780]

Europe PMC Funders Author Manuscripts

Europe PMC Funders Author Manuscripts

33. Allen IV, McKeown SR. A histological, histochemical and biochemical study of the macroscopically normal white matter in multiple sclerosis. J Neurol Sci. 1979; 41:81–91. [PubMed: 438845]

34. Allen IV, McQuaid S, Mirakhur M, Nevin G. Pathological abnormalities in the normal-appearing white matter in multiple sclerosis. Neurol Sci. 2001; 22:141–4. [PubMed: 11603615]

35. Lassmann H, Bruck W, Lucchinetti CF. The immunopathology of multiple sclerosis: an overview. Brain Pathol. 2007; 17:210–8. [PubMed: 17388952]

36. Zeis T, Graumann U, Reynolds R, Schaeren-Wiemers N. Normal-appearing white matter in multiple sclerosis is in a subtle balance between inflammation and neuroprotection. Brain. 2008; 131:288–303. [PubMed: 18056737]

37. Ransohoff RM, Perry VH. Microglial physiology: unique stimuli, specialized responses. Annu Rev Immunol. 2009; 27:119–45. [PubMed: 19302036]

38. Schwartz M, Butovsky O, Bruck W, Hanisch UK. Microglial phenotype: is the commitment reversible? Trends in Neurosciences. 2006; 29:68–74. [PubMed: 16406093]

39. Pitt D, Werner P, Raine CS. Glutamate excitotoxicity in a model of multiple sclerosis. Nat Med. 2000; 6:67–70. [PubMed: 10613826]

40. Fu Y, Sun W, Shi Y, Shi R, Cheng JX. Glutamate excitotoxicity inflicts paranodal myelin splitting and retraction. PLoS One. 2009; 4:e6705. [PubMed: 19693274]

41. Brown DA, Sawchenko PE. Time course and distribution of inflammatory and neurodegenerative events suggest structural bases for the pathogenesis of experimental autoimmune encephalomyelitis. J Comp Neurol. 2007; 502:236–60. [PubMed: 17348011]

42. Jones MV, Nguyen TT, Deboy CA, Griffin JW, Whartenby KA, Kerr DA, Calabresi PA. Behavioral and pathological outcomes in MOG 35-55 experimental autoimmune encephalomyelitis. J Neuroimmunol. 2008; 199:83–93. [PubMed: 18582952]

43. Centonze D, Muzio L, Rossi S, Cavasinni F, De Chiara V, Bergami A, Musella A, D'Amelio M, Cavallucci V, Martorana A, Bergamaschi A, Cencioni MT, Diamantini A, Butti E, Comi G, Bernardi G, Cecconi F, Battistini L, Furlan R, Martino G. Inflammation triggers synaptic alteration and degeneration in experimental autoimmune encephalomyelitis. J Neurosci. 2009; 29:3442–52. [PubMed: 19295150]

44. Lehnardt S. Innate immunity and neuroinflammation in the CNS: The role of microglia in Toll-like receptor-mediated neuronal injury. Glia. 2009; 58:253–63. [PubMed: 19705460]

45. Kerfoot SM, Long EM, Hickey MJ, Andonegui G, Lapointe BM, Zanardo RC, Bonder C, James WG, Robbins SM, Kubes P. TLR4 contributes to disease-inducing mechanisms resulting in central nervous system autoimmune disease. J Immunol. 2004; 173:7070–7. [PubMed: 15557205]

46. Soulika AM, Lee E, McCauley E, Miers L, Bannerman P, Pleasure D. Initiation and progression of axonopathy in experimental autoimmune encephalomyelitis. J Neurosci. 2009; 29:14965–79. [PubMed: 19940192]

47. Nikodemova M, Watters JJ, Jackson SJ, Yang SK, Duncan ID. Minocycline down-regulates MHC II expression in microglia and macrophages through inhibition of IRF-1 and protein kinase C (PKC)alpha/betaII. J Biol Chem. 2007; 282:15208–16. [PubMed: 17395590]

48. Popovic N, Schubart A, Goetz BD, Zhang SC, Linington C, Duncan ID. Inhibition of autoimmune encephalomyelitis by a tetracycline. Ann Neurol. 2002; 51:215–23. [PubMed: 11835378]

49. Giuliani F, Hader W, Yong VW. Minocycline attenuates T cell and microglia activity to impair cytokine production in T cell-microglia interaction. J Leukoc Biol. 2005; 78:135–43. [PubMed: 15817702]

50. Boiko T, Rasband MN, Levinson SR, Caldwell JH, Mandel G, Trimmer JS, Matthews G. Compact myelin dictates the differential targeting of two sodium channel isoforms in the same axon. Neuron. 2001; 30:91–104. [PubMed: 11343647]

51. Rios JC, Rubin M, St Martin M, Downey RT, Einheber S, Rosenbluth J, Levinson SR, Bhat M, Salzer JL. Paranodal interactions regulate expression of sodium channel subtypes and provide a diffusion barrier for the node of Ranvier. JNeurosci. 2003; 23:7001–11. [PubMed: 12904461]

52. Goldin AL. Resurgence of sodium channel research. Annu Rev Physiol. 2001; 63:871–94. [PubMed: 11181979]

Europe PMC Funders Author Manuscripts

Europe PMC Funders Author Manuscripts

53. Kearney JA, Buchner DA, de Haan G, Adamska M, Levin SI, Furay AR, Albin RL, Jones JM, Montal M, Stevens MJ, Sprunger LK, Meisler MH. Molecular and pathological effects of a modifier gene on deficiency of the sodium channel Scn8a (Nav1.6). Hum Mol Genet. 2002; 11:2765–75. [PubMed: 12374766]

54. Novakovic SD, Levinson SR, Schachner M, Shrager P. Disruption and reorganization of sodium channels in experimental allergic neuritis. Muscle Nerve. 1998; 21:1019–32. [PubMed: 9655120]

55. Aboul-Enein F, Weiser P, Hoftberger R, Lassmann H, Bradl M. Transient Axonal Injury in the Absence of Demyelination: A Correlate of Clinical Disease in Acute Experimental Autoimmune Encephalomyelitis. Acta Neuropathologica. 2006; 111:539–47. [PubMed: 16718350]

56. Mathey EK, Derfuss T, Storch MK, Williams KR, Hales K, Woolley DR, Al Hayani A, Davies SN, Rasband MN, Olsson T, Moldenhauer A, Velhin S, Hohlfeld R, Meinl E, Linington C. Neurofascin as a novel target for autoantibody-mediated axonal injury. J ExpMed. 2007; 204:2363–72.

57. Derfuss T, Parikh K, Velhin S, Braun M, Mathey E, Krumbholz M, Kumpfel T, Moldenhauer A, Rader C, Sonderegger P, Pollmann W, Tiefenthaller C, Bauer J, Lassmann H, Wekerle H, Karagogeos D, Hohlfeld R, Linington C, Meinl E. Contactin-2/TAG-1-directed autoimmunity is identified in multiple sclerosis patients and mediates gray matter pathology in animals. Proc Natl Acad Sci U S A. 2009; 106:8302–7. [PubMed: 19416878]

58. Craner MJ, Newcombe J, Black JA, Hartle C, Cuzner ML, Waxman SG. Molecular changes in neurons in multiple sclerosis: altered axonal expression of Nav1.2 and Nav1.6 sodium channels and Na+/Ca2+ exchanger. ProcNatlAcadSciUSA. 2004; 101:8168–73.

59. Black JA, Newcombe J, Trapp BD, Waxman SG. Sodium channel expression within chronic multiple sclerosis plaques. J Neuropathol Exp Neurol. 2007; 66:828–37. [PubMed: 17805013]

60. Waxman SG, Craner MJ, Black JA. Na+ channel expression along axons in multiple sclerosis and its models. Trends PharmacolSci. 2004; 25:584–91.

Europe PMC Funders Author Manuscripts

Europe PMC Funders Author Manuscripts

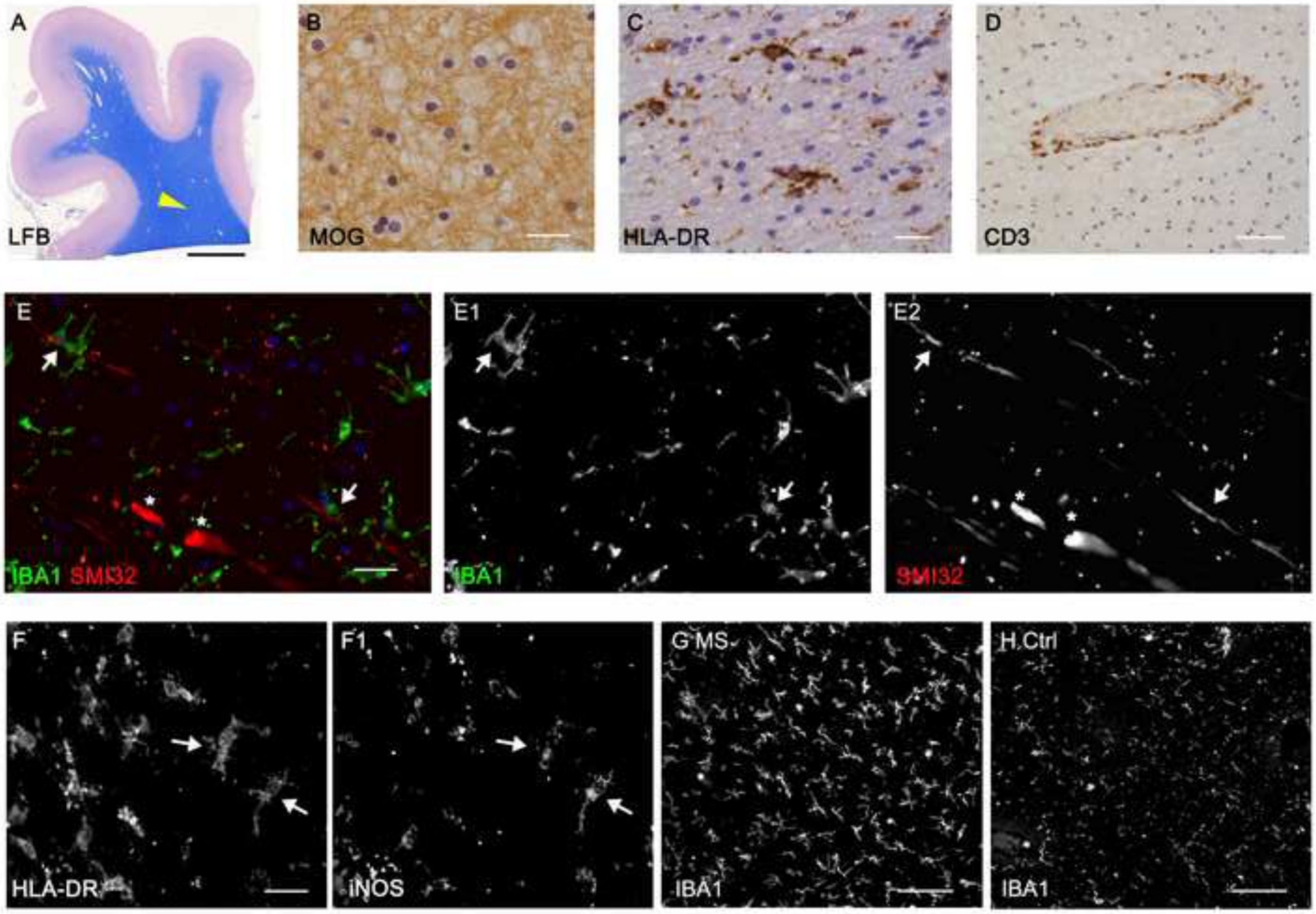

Figure 1.

MS normal appearing white matter is characterised by microgliosis, axon damage and perivascular lymphocytic infiltrates. (A, B) Luxol fast blue histology and MOG immunochemistry of forebrain post-mortem tissue blocks was used to identify normal appearing white matter regions of interest (arrow head in A). (C) HLA-DR$^+$ microglia with an activated morphology were found throughout the normal white matter and CD3$^+$ T-cell infiltrates were restricted to perivascular cuffs (D). (E-E2) Immunostaining with the SMI32 antibody identifies stressed/ damaged axons containing nonphosphorylated neurofilaments morphologically consistent with transections (asterisks) or closely apposed to microglia (IBA1$^+$, arrows). Microglial activation was confirmed by their altered morphology and expression of HLA-DR and iNOS in MS normal white matter (F,F1) and were present at a greater density in comparison to controls (G,H). Ctrl; control, MOG; myelin oligodendrocyte glycoprotein, LFB; luxol fast blue. Scale bars, A= 0.5cm; B, C, E-E2= 20µm; D= 100µm; F-F1= 10µm; G, H= 50µm.

Europe PMC Funders Author Manuscripts

Europe PMC Funders Author Manuscripts

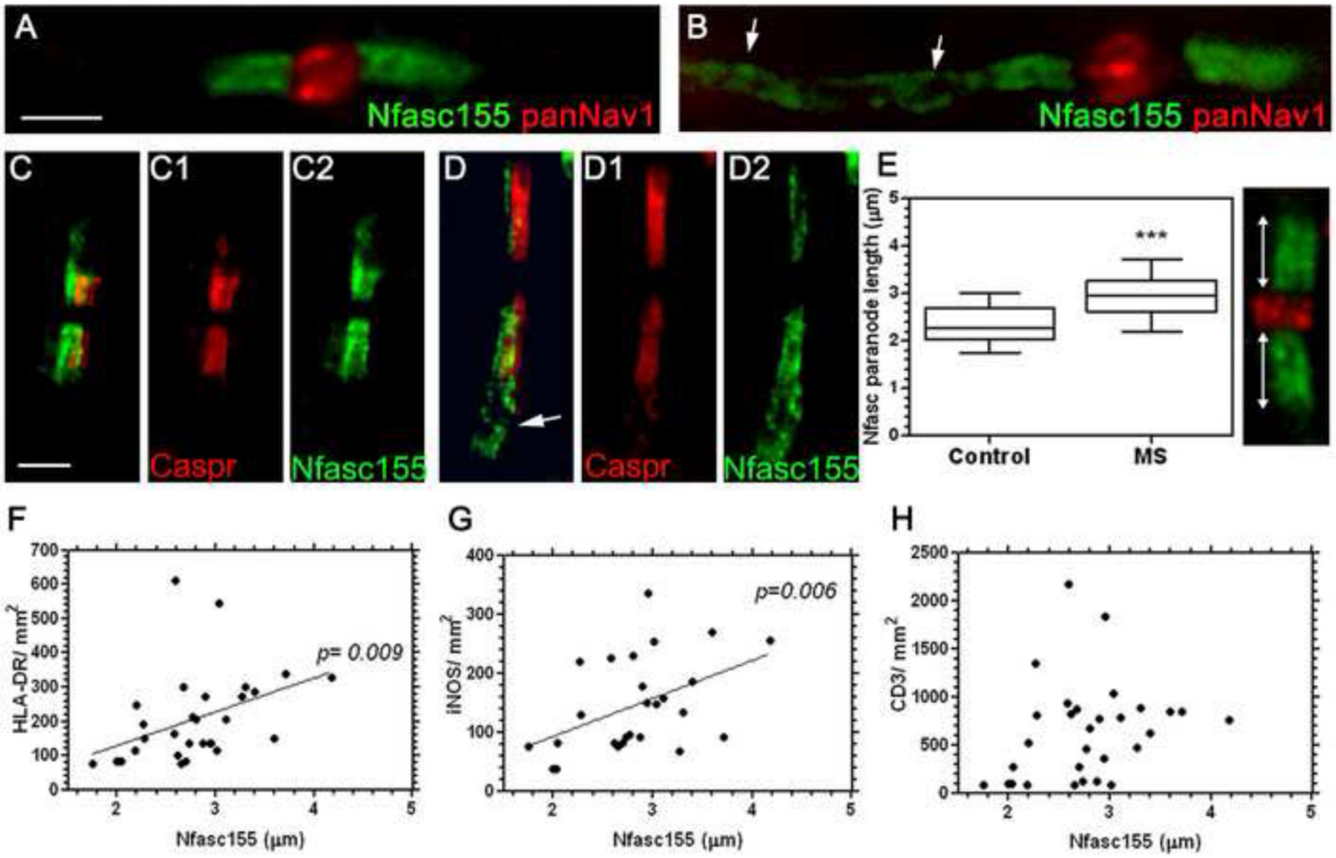

Figure 2.

Paranodal axo-glial disruption in MS normal appearing white matter. (A) Paranodal axo-glial junctions identified by immunostaining for Nfasc155 normally revealed compact paranodal structures separated by Na_V1 channels of the node, although elongated, disrupted structures were noted (arrows in B). (C, D) Paranodal disruption, which takes the form of an elongation along the length of the axon, was noted by an altered expression in Nfasc155$^+$ and Caspr1$^+$ immunostaining (arrow in D). (E) Quantification of single Nfasc155$^+$ structures from control and MS white matter revealed a significant increase in Nfasc155 paranode length in MS (Box plot of mean paranodal lengths per case showing minimum, maximum, interquartile and median values), ***= p< 0.001, Mann-Whitney test. By comparing Nfasc155$^+$ structure length with markers of microglial activation, we found a significant correlation between Nfasc155$^+$ structure elongation and HLA-DR$^+$ microglial density (F) and iNOS expressing microglia (G); but not to the presence of CD3$^+$ T-lymphocytes in the MS tissue (H). Spearman's non-parametric correlation. Ctrl= control. Scale bars, A-D= 2μm; F-H= 50μm; I-I" = 10μm.

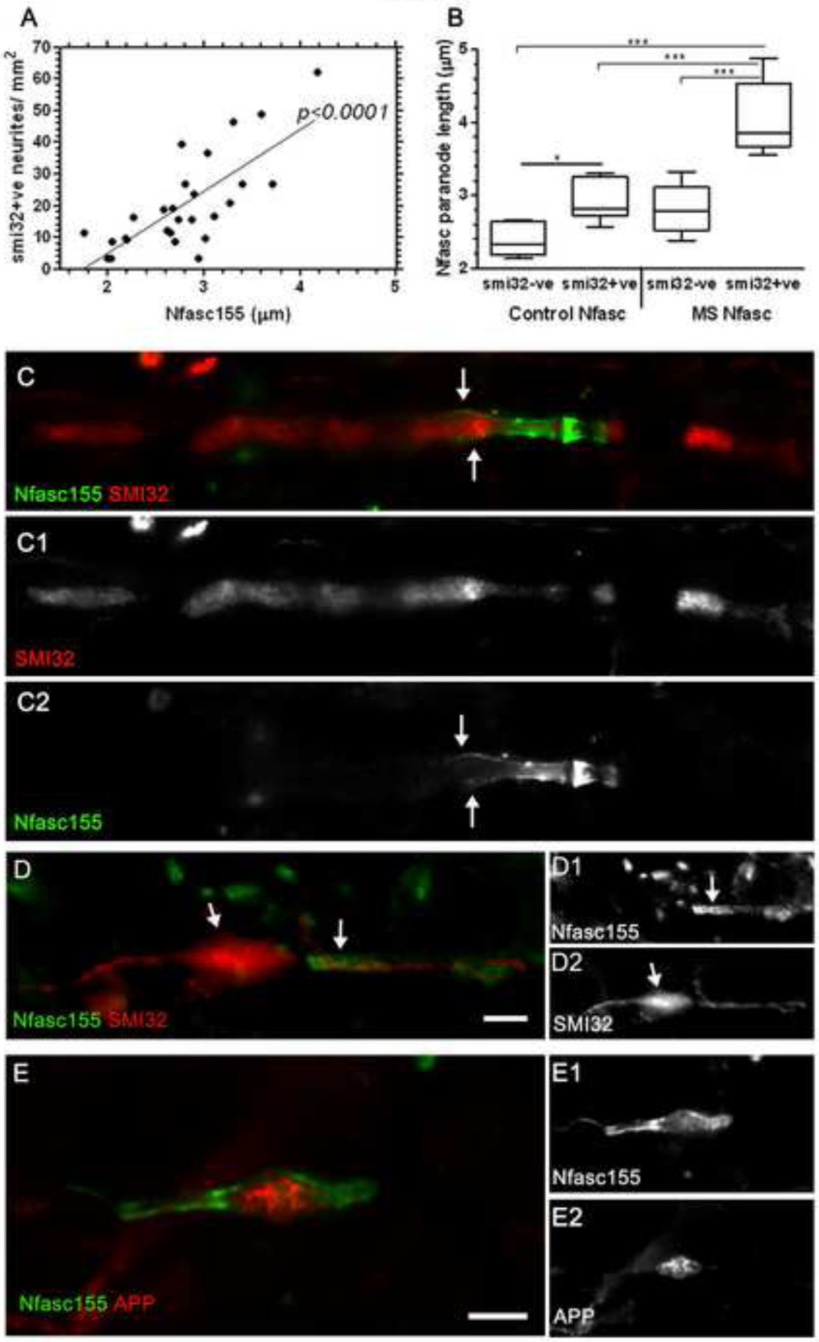

Figure 3.

Paranodal disruption is associated with underlying axonal pathology. (A) Nfasc155$^+$ paranode length correlated with the incidence of SMI32$^+$ axons per NAWM region of interest (Spearman's non-parametric correlation). (B) Quantification of individual Nfasc155$^+$ paranodes revealed an increase in length of those associated with SMI32$^+$ axons in comparison to Nfasc155$^+$ paranodes on SMI32$^-$ profiles (Box plot of mean paranodal lengths per case showing minimum, maximum, interquartile and median values). ANOVA and Bonferroni's multiple comparison post test (* $p<0.05$; *** $p<0.001$). (C-C2), SMI32$^+$

Europe PMC Funders Author Manuscripts

Europe PMC Funders Author Manuscripts

axons associated with disrupted Nfasc155$^+$ paranodes and SMI32$^+$ axonal swellings were noted at nodes of Ranvier (D). (E) Amyloid precursor protein (APP) accumulation is an indicator of axonal pathology and APP was noted in axons of the NAWM that occasionally associated with disrupted nodal profiles. APP, amyloid precursor protein; NAWM, normal appearing white matter. Scale bars, C-F= 2μm; G= 10μm.

Europe PMC Funders Author Manuscripts

Europe PMC Funders Author Manuscripts

Europe PMC Funders Author Manuscripts

Europe PMC Funders Author Manuscripts

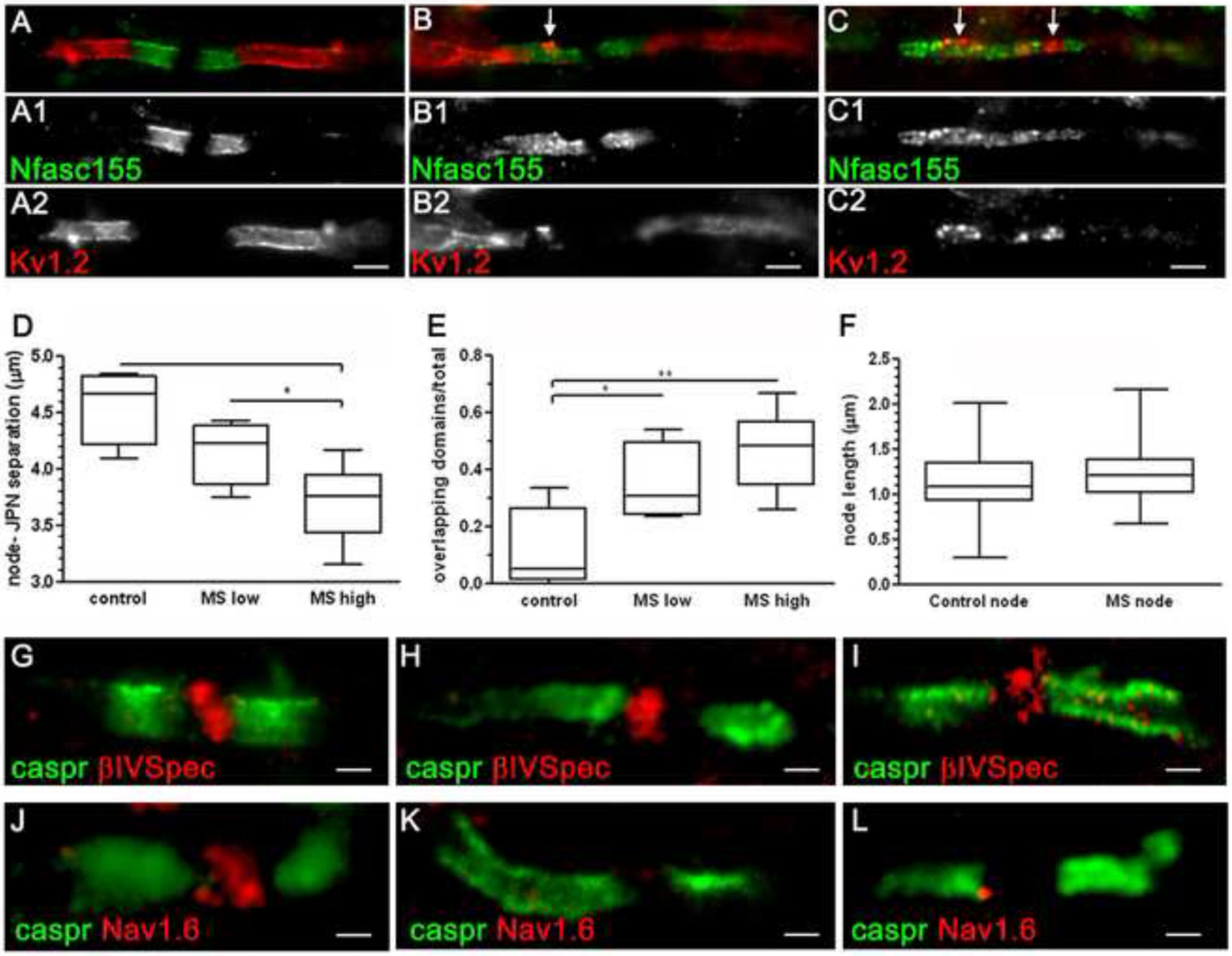

Figure 4.

Microgliosis and paranodal disruption results in the displacement of juxtaparanodal domains and the loss of Na$_V$1.6 expression at nodes. (A-C) K$_V$1.2 that demarcate the juxtaparanodal domains underneath the myelin sheath are normally separated from the node by paranodes (Nfasc155$^+$). Nfasc155$^+$ paranodal junctions with a disrupted appearance frequently coincided with an apparent encroachment of juxtaparanodal K$_V$1 channels (arrows, B, C). MS NAWM was categorised as containing relatively low (MS ‘low’) NAWM inflammation/ axonal pathology or relatively high inflammation/ axonal pathology (MS “high; see methods and Table 1 for details). K$_V$1$^+$ juxtaparanodal profiles were displaced nearer to the node of Ranvier in MS NAWM, with the juxtaparanodal-nodal separation smallest in the MS ‘high’ group (D). Within the same group, the occurrence of overlapping Nfasc155$^+$/ K$_V$1$^+$ domains was greatest. Box plot representing mean values/ case showing minimum, maximum, interquartile and median values. ANOVA and Bonferroni’s post test (D, E; * $p<0.05$; ** $p<0.01$). (E). Quantification of Na$_V$1$^+$ nodal profiles associated with paranodal Nfasc155$^+$ immunolabelling revealed these structures to be unchanged in size between control and MS (F). Na$_V$1 at the node associate with cytoskeletal proteins such as βIV-spectrin that label nodes of Ranvier (G-I). Immunostaining for the $Na_v1.6$ channel subtype revealed instances of attenuated or undetectable staining of nodes with normal and disrupted $Caspr1^+$ paranodes (J-L). NAWM, normal appearing white matter; JPN, juxtaparanode. Scale bars, A-C= 2µm; G-I,K,L= 1µm, J= 0.5µm.

Europe PMC Funders Author Manuscripts

Europe PMC Funders Author Manuscripts

Europe PMC Funders Author Manuscripts
Europe PMC Funders Author Manuscripts

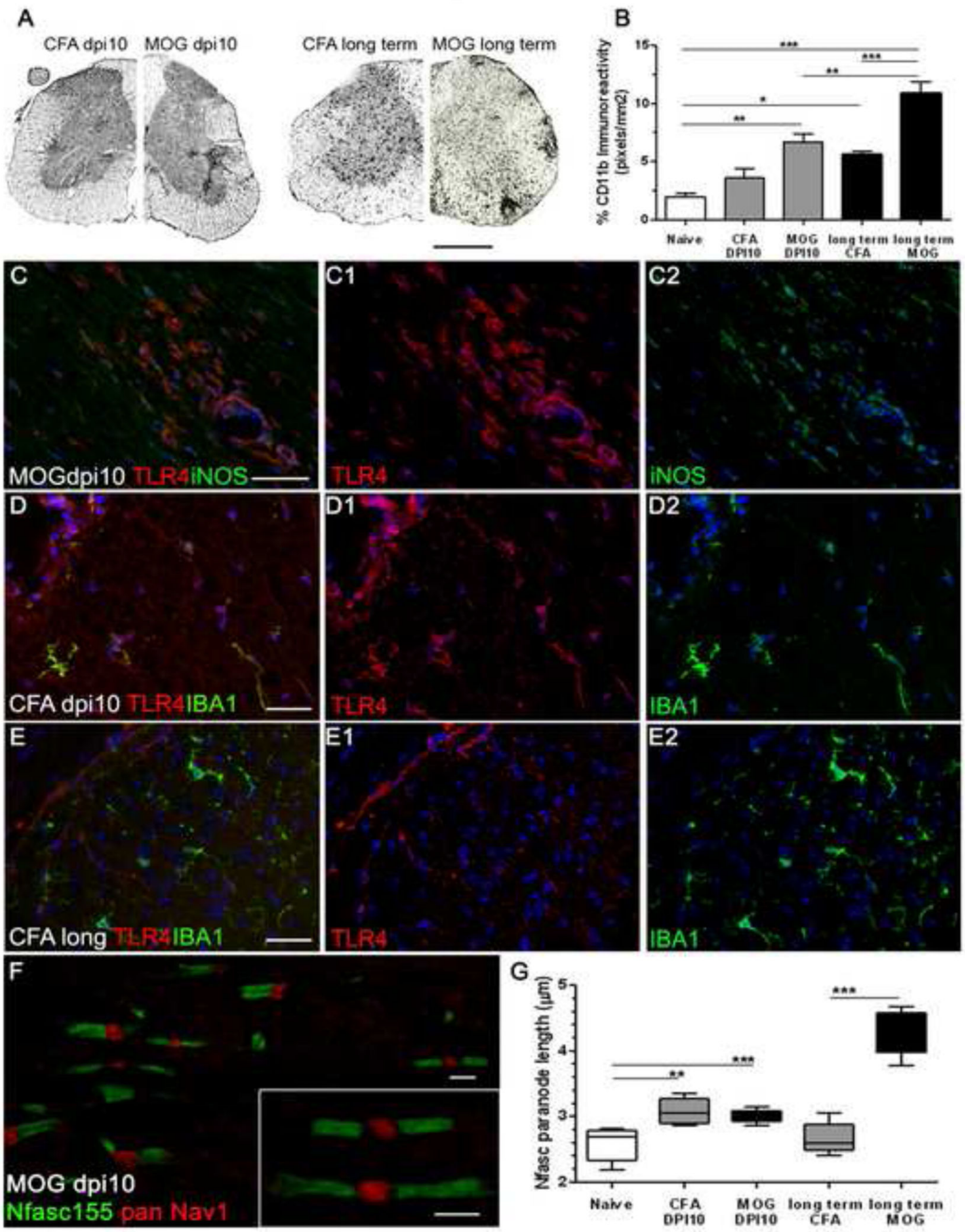

Figure 5.

Microglial inflammation associated with the disruption of paranodal junctions in an animal model of multiple sclerosis. (A,B) Immunohistochemistry for CD11b revealed significant increases in microglial density in transverse sections of spinal cord of MOG$_{35\text{-}55}$ immunised mice at dpi10 (MOG dpi10) and long term CFA and MOG groups (dpi44). ANOVA with Bonferoni's post test (n=5 animals per group). (C-E) MOG immunised animals at dpi10 contained meningeal, perivascular and parenchymal TLR4$^+$ and iNOS$^+$ monocytes/ microglia in lumbar spinal cord. TLR4$^+$ microglia were noted in CFA dpi10 tissue but not in

Europe PMC Funders Author Manuscripts

Europe PMC Funders Author Manuscripts

the CFA long term animals, indicative of temporary microglial activation in this group. (F) Elongated Nfasc155$^+$ paranodes were noted in pre-symptomatic MOG dpi10 tissue (inset) and paranodal elongation was significantly different from naïve in CFA dpi10, MOG dpi10 and long term MOG lumbar spinal cord (G). Nfasc155 changes were reversed in the long-term CFA group. Box plot of mean paranodal lengths per case showing minimum, maximum, interquartile and median values. ANOVA with Bonferoni's post test (n=5 animals per group). *=$p<0.05$, **=$p<0.01$, ***=$p<0.001$. dpi, days post induction. Scale bars, A= 300μm; C-E= 20μm; F= 2 μm.

Europe PMC Funders Author Manuscripts

Europe PMC Funders Author Manuscripts

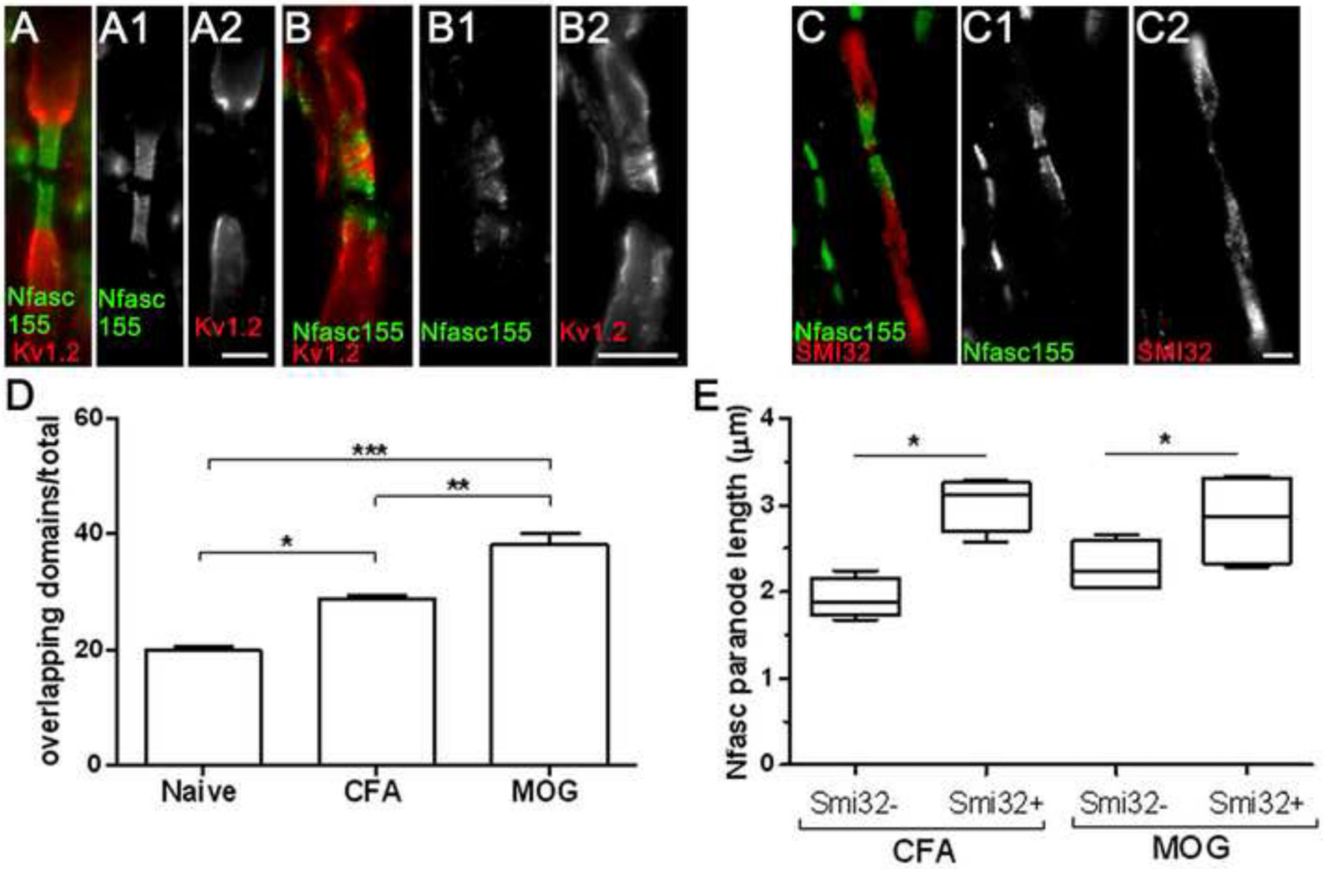

Figure 6.

Paranodal axo-glial disruption in EAE associates with juxtaparanodal re-arrangements and axon stress. (A) Longitudinal sections of lumbar spinal cord white matter contained $K_V1.2^+$ juxtaparanodal and $Nfasc155^+$ paranodal domains located in a non-overlapping conformation. MOG immunised mice at 10dpi frequently presented $K_V1.2^+$ encroachment into disrupted paranodal domains (B). (C) $SMI32^+$ stressed/ damaged axons associated with disrupted $Nfasc155^+$ profiles in both CFA and MOG immunised groups at 10dpi. The incidence of overlapping $K_V1.2$/ Nfasc155 domains were significantly increased in CFA and MOG immunised dpi10 mice in comparison to naïve controls (D; proportion of overlapping K_V1^+ / $Nfasc155^+$ domains of total K_V1^+/$Nfasc155^+$ domains analysed; n=5 per group. ANOVA with Bonferroni post test). (E) Damaged axons ($SMI32^+$) associated with significantly elongated $Nfasc155^+$ paranodal profiles in comparison to $Nfasc155^+$ paranodes upon SMI32-fibres in both CFA and MOG dpi10 groups. (Box plot of mean paranodal lengths per case showing minimum, maximum, interquartile and median values; CFA or MOG group means compared by Mann-Whitney t-test). n=5 animals per group. *=p<0.05, **=p<0.01, ***=p<0.0001. dpi; days post induction. Scale bars A-C= 2μm.

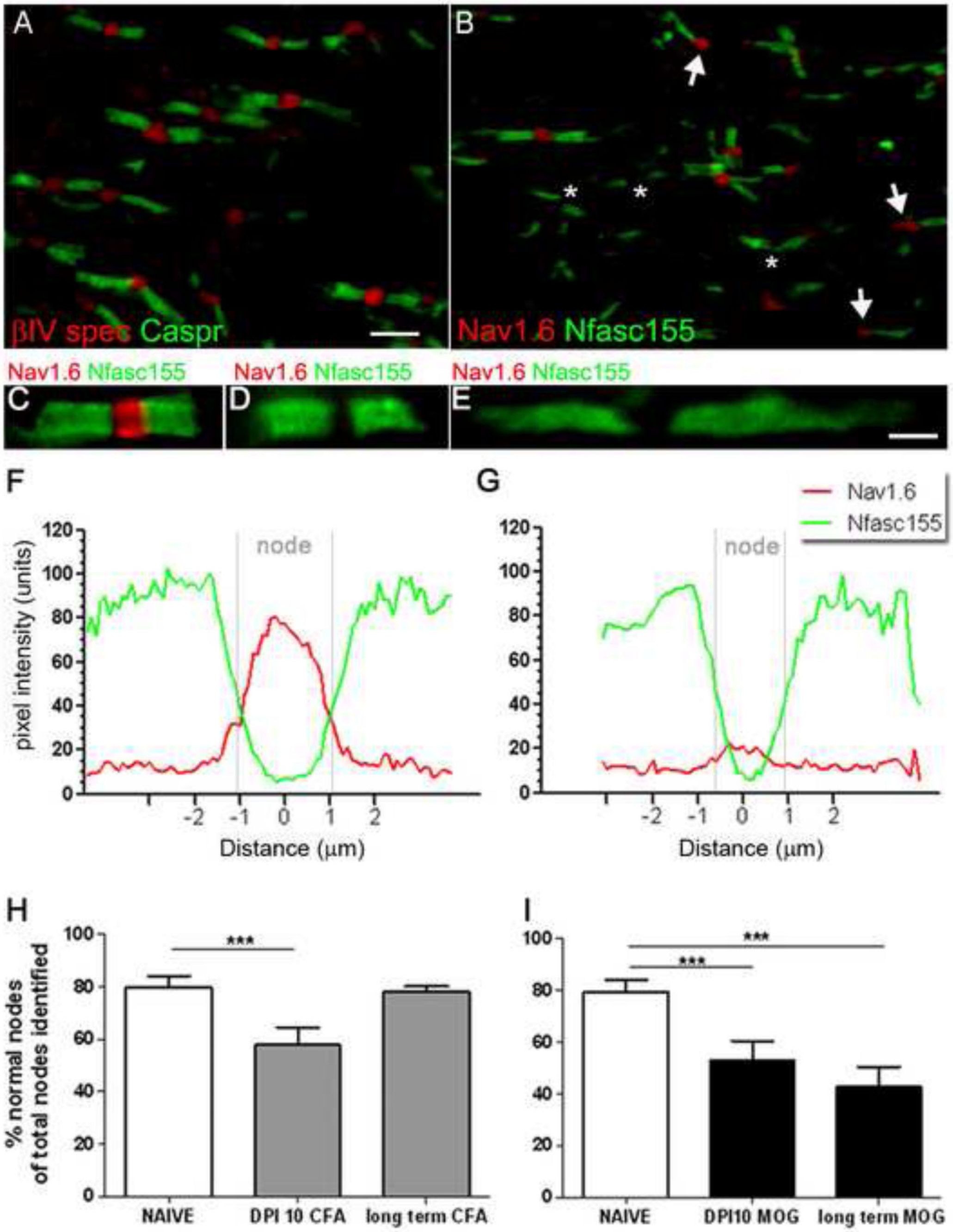

Figure 7.

Disruption of nodal $Na_V1.6$ expression in EAE. (A,B) βIV spectrin$^+$ nodes associated with the vast majority of Caspr1$^+$ paranodes in MOG immunised dpi10 animals. Nodal abnormalities took the form of $Na_V1.6$ negative nodes (asterisks) and heminodes (arrows, B) at Nfasc155$^+$ paranodes. $Na_V1.6^+$ negative nodes were associated with normal appearing and disrupted paranodal profiles (C-E). (F, G) The intensity of Nfasc155 (green line) and $Na_V1.6$ (red line) immunostaining from regular and $Na_V1.6$ negative nodes was calculated by plotting the mean of 20 normal and 20 $Na_V1.6^+$ negative nodes (pixel intensity, 0-255 units),

Europe PMC Funders Author Manuscripts

Europe PMC Funders Author Manuscripts

normalized and averaged from single confocal images. These data confirmed the absence of detectable $Na_v1.6$ at the node. The proportion of aberrant ($Na_v1.6$ negative or $Na_v1.6$ heminodes) nodes were significantly different in MOG and CFA animals at dpi10 (H, I) compared with naïve animals. This trend was reversed in long term CFA animals (H), whilst there was an increased prevalence of aberrant nodes in long term MOG immunised animals compared with naïve controls (I). ANOVA and Bonferroni's post test (***p<0.001). n=5 animals per group. dpi; days post induction. Scale bars A, B=5μm; C-E=2μm.

Europe PMC Funders Author Manuscripts

Europe PMC Funders Author Manuscripts

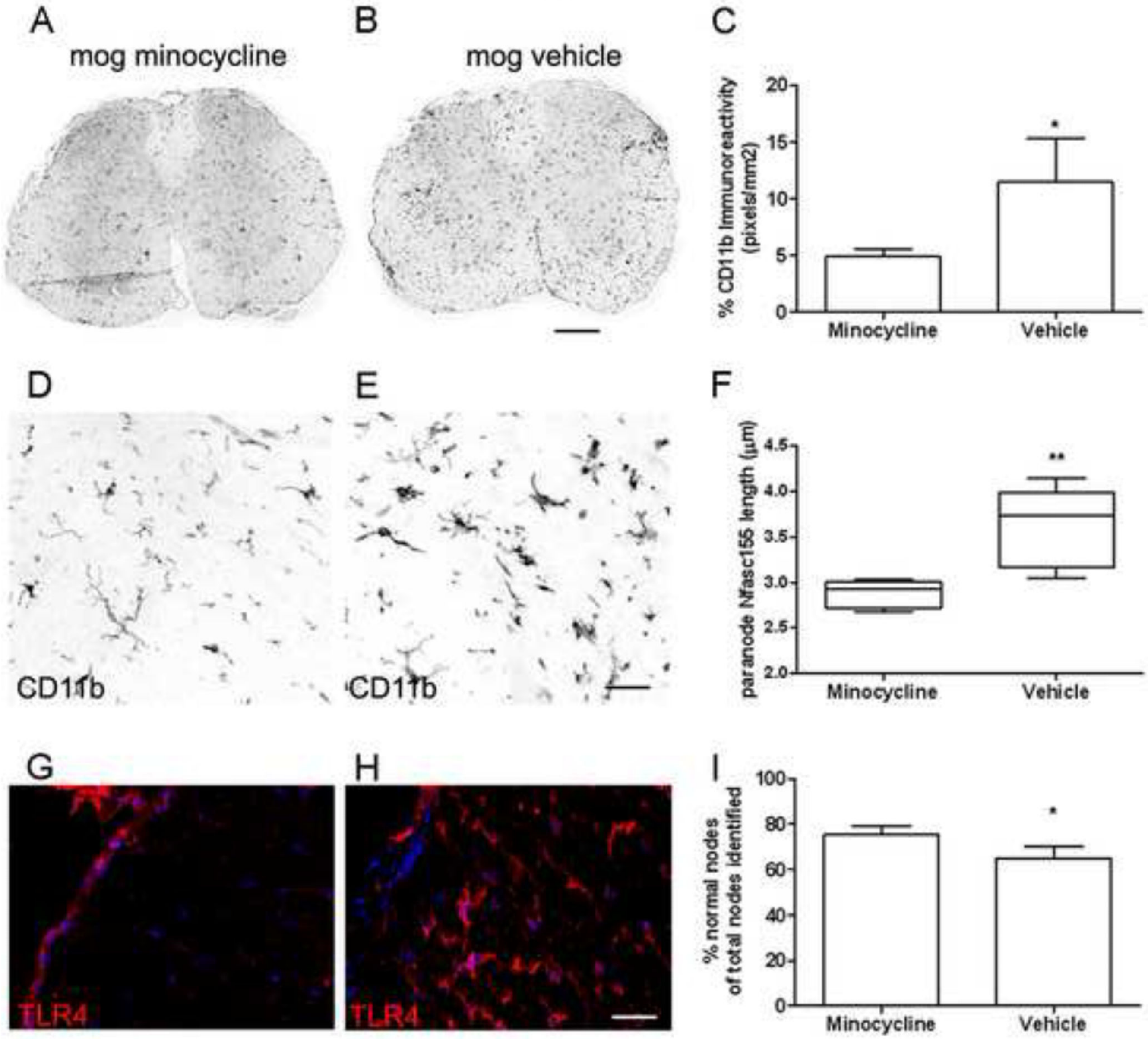

Figure 8.

Administration of minocycline reduced the density of microglial inflammation and abolished disease induced changes at paranodal and nodal units. (A-C) The density of CD11b immunoreactivity (mean signal intensity per animal± sem) in transverse spinal cord was greatly reduced in minocycline treated mice in comparison to vehicle dosed MOG immunised animals. (D, G) Minocycline treated animals contained microglia with a resting morphology that lacked TLR4 expression, in contrast to microglia in vehicle MOG immunised mice (E, H). (F) Nfasc155$^+$ paranode length was increased in vehicle treated animals in comparison to the minocycline group (Box plot of mean paranodal lengths per case showing minimum, maximum, interquartile and median values), whilst the incidence of nodal abnormalities was greater in the vehicle dosed animals (I). n=5 animals per group;

Europe PMC Funders Author Manuscripts

Europe PMC Funders Author Manuscripts

*=$p<0.05$, **=$p<0.01$ Mann-Whitney test. Dpi; days post induction. Scale bars A, B= 200μm, D-H= 30μm.

Europe PMC Funders Author Manuscripts

Europe PMC Funders Author Manuscripts

Table 1

Details of control, multiple sclerosis and Parkinson’s disease cases

Case	*Sex*	*Age yrs.*	*PMD hrs.*	*Disease duration*	*Cause of death*	*Disease course*	*No. of blocks*	*NAWM group*
C005	M	58	14	-	Myocardial infarct	-	1	Control
C014	M	64	18	-	Myocardial infarct	-	1	Control
C020	F	84	24	-	Myocardial infarct	-	1	Control
C025	M	35	22	-	Tongue cancer	-	2	Control
C026	F	78	33	-	Leukaemia	-	1	Control
C030	M	75	17	-	Bronchopneumonia	-	2	Control
C032	M	88	22	-	Prostate cancer	-	1	Control
C036	M	68	30	-	Myocardial infarct	-	1	Control
PDC001	M	76	24	-	Myocardial infarct	-	2	Control
PDC004	M	84	27	-	Not known	-	2	Control
PDC015	F	81	15	-	Oesophageal cancer	-	2	Control
MS015	M	62	24	36	Myocardial infarct	SP	1	MS low
MS079	F	49	7	24	Bronchopneumonia	SP	1	MS low
MS106	F	39	18	21	Bronchopneumonia	PP	1	MS low
Ms109	F	60	22	25	Myocardial infarct	SP	2	MS high
MS136	M	40	10	12	Sepsis	SP	2	MS low
MS179	F	70	20	24	Bronchopneumonia	SP	1	MS high
MS180	F	44	9	18	Bronchopneumonia	SP	1	MS high
MS187	F	57	13	30	Myocardial infarct	SP	1	MS high
MS192	F	78	24	47	Bronchopneumonia	SP	1	MS high
MS200	F	43	20	19	Urinary tract infec	SP	2	MS high
MS229	M	53	13	16	Bronchopneumonia	SP	1	MS high
MS231	F	59	13	27	Bronchopneumonia	PP	1	MS low
MS234	F	39	15	15	Bronchopneumonia	SP	1	MS high
MS235	M	53	14	33	Urinary tract infec	SP	2	MS low
MS237	M	77	19	39	Bronchopneumonia	SP	2	MS low
MS245	M	63	24	25	Bronchopneumonia	SP	2	MS high
MS256	F	53	21	24	Bronchopneumonia	SP	1	MS low
MS273	M	61	24	31	Urinary tract infec	PP	2	MS high
PD010	F	81	21	14	Not known	PDD/ DLB	2	n/a
PD016	F	85	15	18	Bronchopneumonia	PDD	2	n/a
PD017	M	75	28	18	Cerebrovascular disease	PDD	2	n/a
PD021	M	76	21	27	Not known	PD	2	n/a
PD022	F	76	16	10	Myocardial infarct	PD	2	n/a
PD028	M	82	20	18	bronchopneumonia	PDD	2	n/a
35 cases	**17F:18M**	**64.7yrs**	**19.3hr**	**23.8yrs**			**53**	

C, control; NAWM, normal appearing white matter; PMD, post-mortem delay; PP, primary progressive multiple sclerosis; SP, secondary progressive multiple sclerosis; PD, Parkinson’s disease; PDD, Parkinson’s disease with dementia; DLB, Dementia with Lewy bodies.